Nanoscale Res Lett (2010) 5:1788–1794
DOI 10.1007/s11671-010-9712-0

NANO EXPRESS

Phosphor-Free Apple-White LEDs with Embedded Indium-Rich Nanostructures Grown on Strain Relaxed Nano-epitaxy GaN

C. B. Soh · W. Liu · A. M. Yong · S. J. Chua · S. Y. Chow · S. Tripathy · R. J. N. Tan

Received: 28 June 2010 / Accepted: 19 July 2010 / Published online: 1 August 2010
© The Author(s) 2010. This article is published with open access at Springerlink.com

Abstract Phosphor-free apple-white light emitting diodes have been fabricated using a dual stacked InGaN/GaN multiple quantum wells comprising of a lower set of long wavelength emitting indium-rich nanostructures incorporated in multiple quantum wells with an upper set of cyan-green emitting multiple quantum wells. The light-emitting diodes were grown on nano-epitaxially lateral overgrown GaN template formed by regrowth of GaN over SiO_2 film patterned with an anodic aluminum oxide mask with holes of 125 nm diameter and a period of 250 nm. The growth of InGaN/GaN multiple quantum wells on these stress relaxed low defect density templates improves the internal quantum efficiency by 15% for the cyan-green multiple quantum wells. Higher emission intensity with redshift in the PL peak emission wavelength is obtained for the indium-rich nanostructures incorporated in multiple quantum wells. The quantum wells grown on the nano-epitaxially lateral overgrown GaN has a weaker piezo-electric field and hence shows a minimal peak shift with application of higher injection current. An enhancement of external quantum efficiency is achieved for the apple-white light emitting diodes grown on the nano-epitaxially lateral overgrown GaN template based on the light -output power measurement. The improvement in light extraction efficiency, $\eta_{extraction}$, was found to be 34% for the cyan-green emission peak and 15% from the broad long wavelength emission with optimized lattice period.

Keywords Quantum dots · III-Nitride semiconductor · LEDs

C. B. Soh (✉) · W. Liu · A. M. Yong ·
S. J. Chua · S. Y. Chow · S. Tripathy · R. J. N. Tan
Institute of Materials Research and Engineering, A*STAR (Agency for Science, Technology and Research), 3 Research Link, Singapore 117602, Singapore
e-mail: cb-soh@imre.a-star.edu.sg

S. J. Chua
e-mail: elecsj@nus.edu.sg

S. J. Chua
Singapore-MIT Alliance, National University of Singapore, 4 Engineering Drive 3, Singapore 117576, Singapore

Introduction

High efficient group-III nitride-based light emitting diodes (LEDs) have been intensively developed in recent years for various applications such as street and traffic lights, back lighting and for headlights of automobiles. Solid-state lighting would replace conventional light bulbs and will change the way we light the world [1, 2]. InGaN/GaN, multiple quantum wells (MQWs) are often employed as the active layers due to their relatively high recombination efficiency and blue to green III-Nitride LEDs are commercially available. However, III-Nitride LEDs faced severe constraint when we attempt to incorporate high indium content in the materials due to large lattice mismatch (11%) between InN and GaN [3]. This leads to spinodal decomposition once InN content reaches a critical limit ($\sim$30%) [4]. The conventional white III-Nitride LEDs generated from phosphor coating have the disadvantages of having poor color rendering index, low yield issues in production and reduced thermal stability [5]. Pioneering work to generate phosphor-free white light was done by Damilano et al. [6] and Yamada et al. [7] by having In_xGa_{1-x} N/GaN quantum wells (QWs) of different indium compositions. Recent work by Huang et al. made use of prestrained InGaN well layer to generate white light [8] while Funato et al. has demonstrated a polychromatic

emission (inclusive of white) from LEDs using micro-structured multifaceted quantum wells [9]. Nanostructures, especially III-As-based quantum dots are a subject of wide variety of studies ranging from fundamental physics, quantum electrodynamics [10] to quantum information and computing [11, 12]. InGaAs/GaAs, quantum dots system with high uniformity has been generated on AlGaAs, which demonstrated narrow linewidth and improvement in excitons confinement [13]. III-Nitride quantum dots have also been applied by Chua et al. [14], not to generate narrow linewidth but to have a broad emission spectrum covering from 400 to 700 nm to mimic white (daylight) emission. However, there is still a need to improve on the light extraction efficiency due to total internal reflection, limiting the amount of light which can escape from the LEDs surface [15]. Various patterning techniques have been employed to enhance light extraction from LEDs, which includes surface roughening [16], geometric modification [17] and use of photonic crystals [18, 19].

Nanostructures and photonic crystals have been created by deposition into patterned substrates produced by conventional lithographic approaches such as e-beam lithography, interference lithography or X-ray lithography [20, 21]. These lithography approaches enable precise control of the spacing and dimensions of the nanostructures but the techniques are limited by high cost and low throughput. On the other hand, patterning based on self-organization technique such as the self-ordered aluminum oxide template enables the fabrication of arrays of nanostructures over a large area [21]. Earlier work has reported on the advantages of using nano-air bridge GaN template, which includes threading dislocation reduction and strain relaxation in subsequent InGaN/GaN MQWs or InN quantum dots grown [22, 23]. In this paper, we demonstrate the growth of InGaN/GaN LEDs incorporating indium-rich InGaN nanostructures on the nano-epitaxy lateral overgrown GaN template. Photoluminescence show enhanced peak intensity and higher activation energy for the multiple quantum wells grown on the nano-epitaxy lateral overgrown GaN template. Structural analysis of samples with embedded nanostructures and conventional InGaN/GaN well was carried out by scanning electron microscope (SEM).

Experimental

Preparation of the Nano-ELO GaN Template

To generate the nano-epitaxially lateral overgrown (ELO) air bridge GaN template, a layer of 1.0 μm thick aluminum is first e-beam deposited on 200 nm SiO_2 coated undoped GaN grown on sapphire substrate. The alumina mask was formed by a two-step anodization process carried out in 0.3M oxalic acid at 2°C with an injection voltage of 60 V. After the first anodization step, the sample was immersed in H_2CrO_4 acid at 60°C for 25 min to remove the oxide, leaving behind self-ordered pattern of pits for a subsequent anodization step in oxalic acid. A regular array of nanopores is generated on the alumina template as shown in Fig. 1a after the pores are enlarged in 5wt % of H_3PO_4, which serve as chemical etchant for alumina. Inductively coupled plasma (ICP) etching in CHF_3 ambient is done to

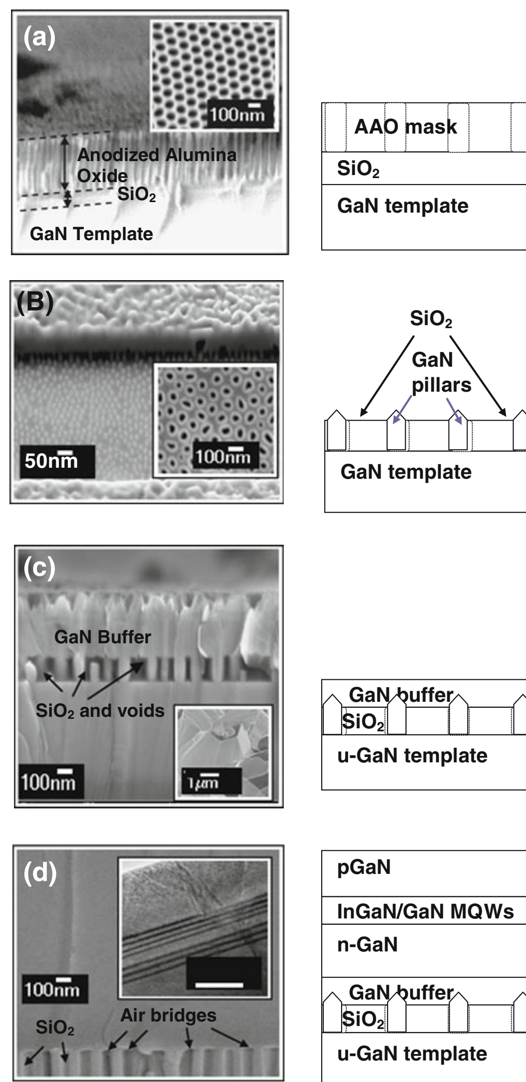

Fig. 1 Cross-section and plane view SEM images of GaN undergoing anodization to generate nano-ELO GaN structures. **a** SEM image of the anodized alumina oxide on GaN coated with a SiO_2 film **b** SEM image after FIB to expose the transfer of the self-ordered patterned site on SiO_2 film with subsequent growth of GaN pillars from these nanopores on SiO_2 **c** re-growth of a thin buffer GaN on the nanopores SiO_2 film **d** Lateral overgrowth to generate strain relaxed GaN template for subsequent growth of the multiple quantum wells and LEDs structures

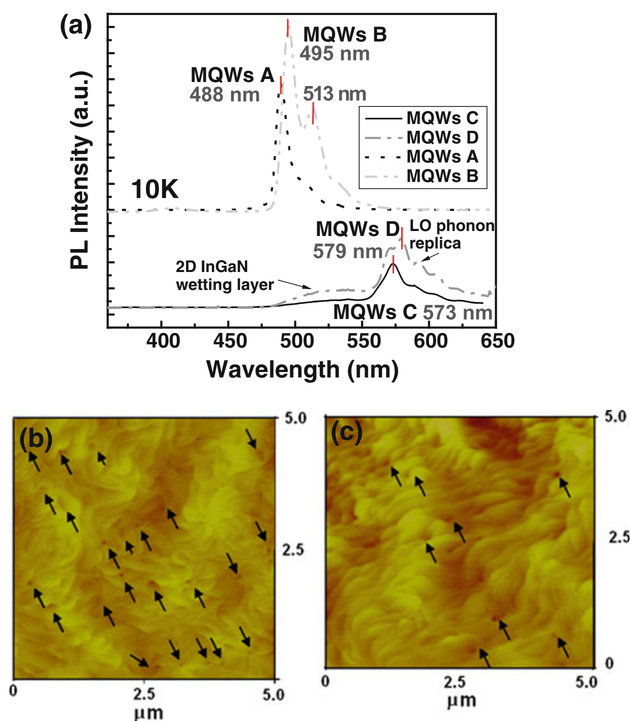

Fig. 2 **a** Low temperature PL spectra of the InGaN/GaN multiple quantum wells at 10 K; MQWs A and B with structures on GaN and nano-ELO GaN template; MQWs C and D with indium-rich nanostructures incorporation in InGaN/GaN structures on GaN and nano-ELO GaN template. AFM plan view images of regrowth **b** strain relaxed GaN on nanopore SiO_2 template **c** GaN on conventional GaN layer. (The *arrows* points to the pits generated on the layers)

etch the underlying SiO_2 to create nanopores before the alumina mask was removed with chemical acid. Figure 1b shows the tilted view of the SiO_2 mask after the top regrown GaN layers were removed by focused ion beam. The nanopores generated on the 200 nm thick SiO_2 film have a diameter of 120–130 nm and a lattice period, **a** of 240–250 nm. GaN pillars are generated from the nanopores as shown in Fig. 2b. There is the tendency for nucleation of GaN nucleated islands to take place from the GaN surface rather than the sidewalls of SiO_2 during regrowth.

Growth of MQWs and LEDs on the Nano-ELO GaN Template

The *u*-GaN sample used for the preparation of the nano-ELO GaN template was grown by metalorganic chemical vapor depositions (MOCVD) at 1,020°C with trimethylgallium (TMGa) and NH_3 gas serving as the precursors for Ga and N, respectively, at a chamber pressure of 500 Torr. A 200 nm thick GaN buffer layer was then regrown on the patterned u-GaN template at 1,020°C as shown in Fig. 1c. To promote lateral overgrowth, the TMGa flow rate was reduced from 90 to 30 sccm, and the chamber pressure was lowered to 200 Torr. The inset of Fig. 1c shows the formation of nucleation islands of GaN over the nanopores of SiO_2 with size of $\sim$2.0 μm and a root mean square roughness of $\sim$11.7 nm. The pressure was then increased to 500 Torr to grow the additional $\sim$2 μm thick *n*GaN as shown in Fig. 1d.

To study the optical emission from InGaN/GaN multiple quantum wells (MQWs) grown on different GaN templates and to achieve enhanced indium incorporation in the InGaN nanostructures embedded in the well layer, four MQWs samples were grown with sample B and D on nano-ELO GaN template while the MQWs of sample A and C were grown on conventional GaN template. Sample A and B are conventional InGaN/GaN MQWs grown at chamber temperature of 755°C while Sample C and D have embedded InGaN nanostructures in the well layer with a growth temperature of 745°C. In sample C and D, 3 periods of InGaN/GaN MQWs were grown with dimensions of 4/10 nm, respectively. Each well consists of a wetting InGaN layer, 1 nm thick grown with TMI flow rate of 24 μmol/min and designated as α-layer. After the growth of the α-layer, TMG flow was switched off allowing only TMI to flow (also known as TMI treatment) for 12 s followed by the growth of a 3 nm thick InGaN, designated as β-layer. The trimethylindium (TMIn) flow for theβ-layer was kept at 70 μmol/min. The InGaN well layer, i.e. the α- and β-layers, were grown at a temperature of 745°C. The detailed growth structures and characterization of these InGaN nanostructures have been reported elsewhere [24]. For the generation of the phosphor-free apple-white InGaN/GaN LEDs, the active emitting region consisting of indium-rich nanostructures incorporated MQWs giving a broadband long wavelength emission stacked with four periods of InGaN/GaN MQWs without embedded nanostructures, and thickness is kept at 3/10 nm. A 25 nm thick electron blocking p-$Al_{0.25}Ga_{0.75}N$ layer was then grown on top of the MQWs followed by a 200 nm thick *p*-GaN layer, and the TEM image of the LEDs with stacked MQWs is as shown in inset of Fig. 1d. The structures of the samples are summarized in Table 1.

Table 1 Tabulation of the sample structures and the type of template used

	Conventional GaN	Nano-ELO template
Conventional InGaN/GaN QWs	A	B
indium-rich nanostructures incorporated InGaN/GaN QWs	C	D
LEDs with Stacked MQWs	E	F

Results and Discussion

Determination of the Optical Properties of MQWs

The external quantum efficiency (η_{ext}) of the LEDs is influenced by its internal quantum efficiency (η_{int}) and light extraction efficiency (η_{extr}). The internal quantum efficiency of the LEDs is dependent on its materials properties and can be evaluated by temperature-dependent photoluminescence spectra. Figure 2a shows the low temperature PL spectra for the MQWs taken at 10 K. Strong PL emission around 495 nm is observed from the sample B grown on nano-ELO GaN template while emission peak at ~513 nm is due to its LO phonon replica. The dominant PL emission from sample B is about 1.5 times higher in terms of its integrated intensity when compared to sample A grown on the conventional GaN template due to reduction in the density of defects such as the screw and the edge dislocations in the regrown GaN. This is similar to the ELOG GaN growth process where SiO_2 is used as the mask. Based on the pits counts from the 5 × 5 µm AFM image of conventional GaN as shown in Fig. 2b, (where no of pits, n_s ~18), the density of threading dislocation is estimated to be ~6.8×10^8 cm^{-2} with a separation of ~600 nm [25]. Since the average spacing between the nanopores is about 100–110 nm, this implies that the SiO_2 mask serves as an effective blocking layer for the propagation of threading dislocations. With regrowth of GaN on nanopores, the threading dislocation density has been reduced to 1.2×10^8 cm^{-2} The surface of the 2.0 µm thick *n*-GaN on nano-ELO GaN template gives a RMS roughness of 0.32 nm when compared to 0.29 nm for conventional GaN template.

We observed a redshift in the peak emission of sample B from that of sample A due to the stress relaxation of the GaN grown on the nano-ELO GaN, which contributes to the greater ease for incorporation of indium in the InGaN well layer. For the indium-rich InGaN nanostructures incorporated in the multiple quantum wells, a redshift is observed in the peak position of the broadband emission from 573 nm of sample C to 579 nm for sample D. The samples were grown on the conventional GaN and nano-ELO GaN template, respectively. The shoulder emission at the higher wavelength side corresponds to the LO phonon replica [26]. The enhancement in the integrated intensity is only 1.3 times after eliminating the emission from the InGaN wetting layer.

Figure 3 shows the temperature-dependent PL measurement carried out for the sample A, and the inset gives the Arrhenius plot of the integrated PL intensity of the emission spectra versus the measurement temperature for the respective samples. At low temperature from 4 to 100 K, the emission is dominated by strong InGaN emission peak. As

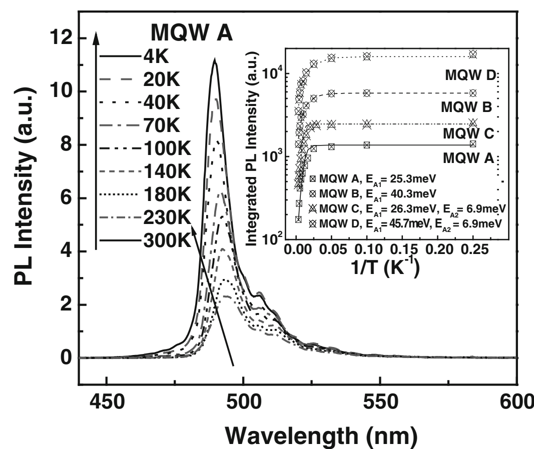

Fig. 3 Temperature varying PL spectra for MQWs A with inset giving the Arrhenius plot for the multiple quantum wells sample

temperature further increases, higher thermal energies cause the activation of the non-radiative recombination centers in the film, and thermal quenching of the InGaN peak emission is observed. By fitting the experimental data of the integrated PL intensity as a function of temperature using the Arrhenius equation,

$$I(T) = \frac{I_O}{[1 + C_1 \exp(-E_{A1}/\kappa T) + C_2 \exp(-E_{A2}/\kappa T)]} \quad (1)$$

the activation energies of the non-radiative recombination centers, E_{A1} for sample A and B are found to be 25.3 and 40.3 meV. This is attributed to capture of carriers by extended defects, in particular the dislocations in GaN substrate. The higher value for E_{A1} for sample B is due to the reduction in threading dislocations which leads to a higher barrier for carrier capture by threading dislocations. For sample C and D, best fitting of the Arrhenius plot is obtained with two activation energies, with E_{A1} at 26.3 meV and E_{A2} at 6.9 meV for Sample C and E_{A1} at 45.7 meV and E_{A2} at 6.9 meV for Sample D. The additional activation energy, E_{A2} corresponds to the thermal delocalization of excitons, which arises from atomic well width fluctuation at the interface of the InGaN well/GaN barrier with embedded indium-rich nanostructures. At low temperature (4–100 K), the luminescence of the sample arises from the localized quantum like states of the indium-rich InGaN nanostructures, which has a higher efficiency than conventional InGaN/GaN MQWs. Excited carriers from the GaN film tend to relax and recombine at these quantum-dot-like states. With increasing temperature, the non-radiative recombination centers are activated and delocalized excitons start to dominate the emission from the multiple quantum wells. The integrated PL intensity decreases more rapidly as shown in Arrhenius plot when the temperature exceeded 140 K. Considering the effect of the non-radiative recombination centers to be negligible at

4 K and taking the internal quantum efficiency to be almost 100% in this temperature regime, the ratio of the integrated PL intensity at 4 K, I_{4K} and 300 K, I_{300K} can be used to estimate the internal quantum efficiency at 300 K. I_{300K}/I_{4K} is 0.26 for Sample A while it is 0.30 for Sample B. The growth on the compressive stress relaxed nano-ELO GaN template with reduction in threading dislocation density contributed to higher internal quantum efficiency of the InGaN/GaN active region. The improvement in the internal quantum efficiency, η_{int} is 15%. The estimation of the internal quantum efficiency is not done for the Sample C and D due to complex nature of emission.

Morphological Studies of the InGaN/GaN MQWs

Figure 4 shows the tapping mode atomic force microscopy (AFM) image of the surface morphology of the quantum well sample on the regrown *n*-GaN on conventional and nano-ELO GaN template. The formation of indium-rich InGaN quantum dots (QDs) after TMIn treatment on the InGaN wetting layer (α layer) of conventional GaN and nano-ELO GaN template is as shown in Fig. 4a and b, respectively. N_2 is used as the carrier gas to slow down the diffusion of indium adatoms, and the reduction in the atomic diffusion of indium enhances the Stranski–Krastanow (SK) growth of InGaN quantum dots. Coupled with the higher continuous flow of NH_3 at 18 slm (standard liters per minutes) when compared to conventional InGaN well growth (12 slm), a higher amount of N interacts and forms bonds with impinging indium at Ga sites of the α-layer. This explains the formation of indium-rich InGaN quantum dots of size ~25 nm in diameter and ~1.3 nm in height with a density of $\sim 8 \times 10^9$ cm^{-2} on conventional GaN template. On the other hand, the indium-rich InGaN quantum dots on α-InGaN layer of nano-ELO GaN template is of bigger dimension and lower density; ~34 nm in diameter and ~1.2 nm in height with a density of $\sim 2.4 \times 10^9 cm^{-2}$ as shown in Fig. 4b. The growth of the quantum dots preferably took place at the step contours of the α-InGaN layer/n-GaN on nano-ELO GaN template. These quantum dots are recessed into the undulated surface and appeared to be levelled with the α-InGaN surface. This explained their lower height of 1.0 nm (than expected) when compared to 1.2 nm for quantum dots on α-InGaN layer/n-GaN of conventional GaN template. The InGaN quantum dots were then capped with a 3.0 nm InGaN well, *β* layer, with the NH_3 flow rate reduced to 12 slm to promote layer by layer growth. Figure 4c shows the AFM image of sample C after the growth of the *β* layer, with the embedded InGaN quantum dots. The InGaN quantum dots clustered and formed nanostructures due to layer growth of the InGaN over the InGaN QDs.

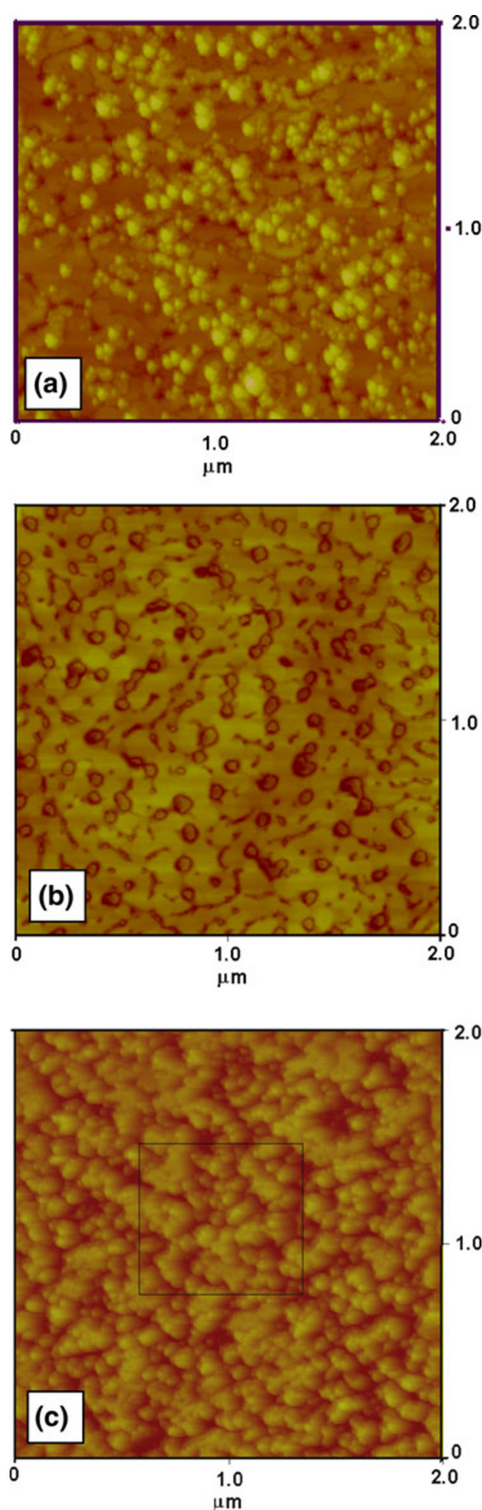

Fig. 4 AFM image of indium-rich InGaN quantum dots (QDs) deposited on the InGaN wetting layer using overgrown GaN on **a** conventional GaN and **b** nano-ELO GaN template. **c** A single quantum well of sample C with clusters of InGaN nanostructures formed by layer growth of the InGaN well layer which wets the quantum dots. The RMS roughness is ~0.82 nm in the *square box* defined

Electroluminescence Study of the LEDs Grown on Nano-ELO GaN Template

To generate apple-white LEDs, a stacked MQWs structures made up of MQWs with embedded nanostructures followed by conventional InGaN/GaN MQWs were grown on GaN (sample E) and nano-ELO GaN template (sample F) before it was capped with a 200 nm thick p-GaN. Figure 5a shows the comparison between the electroluminescence spectrum of LEDs sample E and F with injection current of 20 and 80 mA. Gaussian fitting was carried out for the electroluminescence spectra and two dominant peaks, P1 and P2 were identified. Peak P1 is from the conventional InGaN/GaN MQWs emission and P2 peak emission is from the InGaN nanostructures. As injection current increases from 20 to 80 mA, there is little shift in the EL peak P1, only 0.6 nm (for sample F) and 1.6 nm (for sample E), illustrating that the piezoelectric field effect is low for the green emitting MQWs layer. The peak shift with higher injection current is smaller for growth on the nano-ELO GaN template when compared to conventional GaN due to relaxation of strain. On the other hand, for EL peak P2, there is a significant shift by 10 nm (for sample E) when compared to 3 nm (for sample F). It is known that there exists a strong piezoelectric field in InGaN/GaN well. In the case of indium-rich InGaN nanostructures or quantum dots, this effect will be more enhanced due to larger lattice mismatch of high indium composition InGaN nanostructures with GaN barrier. This causes the band structures of the InGaN/GaN quantum wells (with embedded indium nanostructures, sample C) to bend and leads to a reduction in its PL intensity as shown in Fig. 3a when compared to conventional InGaN/GaN quantum wells, sample A. However, for growth of the LEDs structures using the nano-ELO GaN template, sample F, the blueshift of EL peak P2, with increase in injection current is only minimal due to strain relaxation on the overgrown GaN layer.

To evaluate the light output performance of the LEDs, Newport Optical Power Meter with a UV detector (of bandpass filtering from 200 to 1,100 nm) is used to measure the relative light output power with injection current. The measurement was carried out at the wavelength of the EL peak, P1 and P2 obtained from the EL spectra of the LEDs in Fig. 5a. Figure 5b shows the light output performance of sample E and F for EL peak, P1 and P2 with increase in injection current. In both cases, LEDs from sample E emits with a higher intensity for both P1 and P2. There is an enhancement in light output power by 1.55 times for P1 and 1.31 times for P2 with an injection current of 80 mA. The difference in the value suggests that the array of GaN nanorods with diameter of 120–130 nm, grown in the nanopores of SiO_2 mask with period ~240–250 nm is more effective in enhancing the light

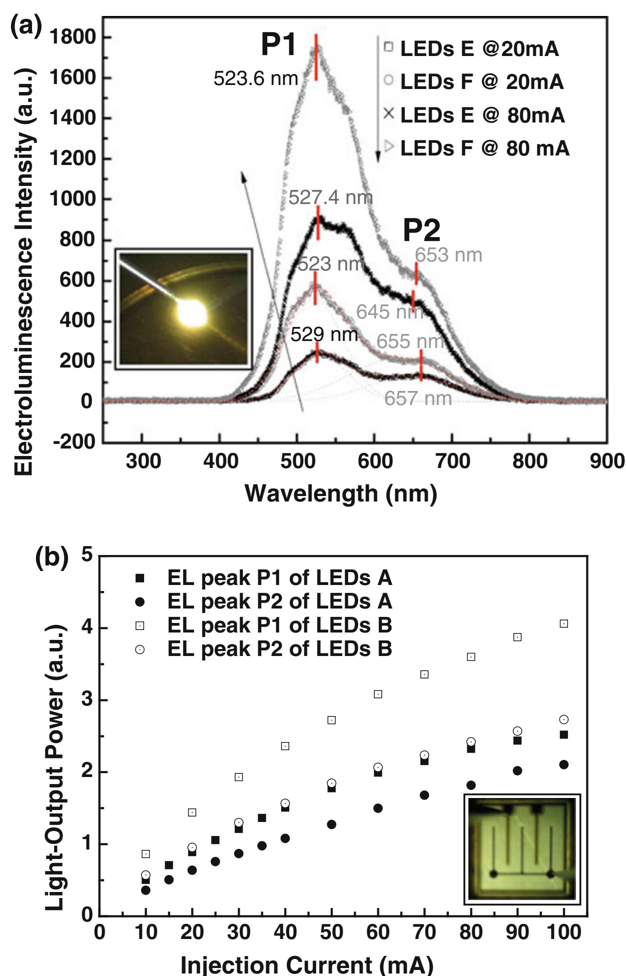

Fig. 5 **a** Electroluminescence (EL) spectra of the LEDs with the stacked MQWs structures grown on conventional GaN template (LEDs A) and on nano-ELO bridge GaN template (LEDs B) with injection current at 20 and 80 mA. Inset shows the emission from the LEDs die on the I–V probe stage **b** Light output power with increasing injection current for EL peak P1 and P2 for LEDs A and B with the image of the LEDs die from optical microscope

extraction for emission wavelength, λ_{P1} ~520 nm than λ_{P2} ~650 nm. The external quantum efficiency, η_{ext} of the multiple quantum wells, is given by $\eta_{ext} = \eta_{extraction} \times \eta_{int}$, where $\eta_{extraction}$ is the light extraction efficiency with embedded nano-ELO GaN template. Since the improvement in η_{int} has been approximated to be 15%, this gives an enhancement in light extraction efficiency, $\eta_{extraction}$ of ~34% for P1 and 14% for P2. Simulation of light extraction with embedded photonic structures consisting of SiO_2 pillar and [27] emission profile with surface patterning [19] have been done for GaN-based LEDs sample. The vertical emission profile for light extraction and enhancement is obtained near the second order diffraction condition, $a/\lambda = 0.50$ where 'a' corresponds to the lattice period and λ is the wavelength of emission. With our emission wavelength peak at λ_{P1} ~520 nm and λ_{P2} ~650 nm, the

lattice period of a ~240–250 nm will give a higher enhancement for emission peak P1 with $a/\lambda_{P1} \sim 0.47$ when compared to broad emission peak, P2 with $a/\lambda_{P1} \sim 0.37$. As the patterns are not perfectly uniform, several of the neighboring nanopores have merged as shown in Fig. 1c. However, there is a substantial degree of periodicity, and the enhancement would also be due to scattering of light from the embedded SiO_2 mask.

Conclusions

In summary, the use of nano-ELO GaN template for growth of LEDs is effective in improving the light output performance of the LEDs through improvement of internal quantum efficiency through the reduction of threading dislocations and stress relaxation. This enhances the indium incorporation in InGaN well layer and also lowers the piezoelectric field in the MQWs layer with a minimal shift in its MQWs emission wavelength with higher injection current for the LEDs grown on the nano-ELO GaN template. Localization of carriers for indium-rich nanostructures incorporated in the MQWs is observed on nano-ELO and conventional GaN templates due to well width fluctuation and localized strain regions at the interface of the GaN barrier/GaN well. The incorporation of the indium-rich nanostructures enables the emission spectrum of the MQWs to be pushed to a longer wavelength which stacked with a conventional cyan emitting InGaN/GaN, MQWs gives the apple-white LEDs. The periodicity of the embedded nano-ELO GaN template enables an enhancement in the light extraction with optimization of the lattice spacing and dimension of the nanopores.

Acknowledgments This work was supported by the IMRE, A*STAR funding under the SSL core project, IMRE/09-1P0604. The authors are grateful for the funding and also the support by SNFC group in IMRE for the use of characterization/fabrication tools.

Open Access This article is distributed under the terms of the Creative Commons Attribution Noncommercial License which permits any noncommercial use, distribution, and reproduction in any medium, provided the original author(s) and source are credited.

References

1. Navigant Consulting, Inc. Radcliffe Advisors and SSLS, Inc, March 2008 Solid State Lighting Research and Development, Mutli-Year Program Plan FY'09-FY'14 32–36
2. R. Mueller-Mach, G. Meuller, M. Krames, T. Trottier, IEEE J. Sel. Top. Quantum Electron **8**, 339 (2002)
3. B. Gil, *Group III-Nitride Semiconductor Compounds, Physics and Application*, **4** 127 (Clarendon Press, Oxford, 1998)
4. N.A. El-Masry, E.L. Piner, S.X. Liu, S.M. Bedair, Appl. Phys. Lett. **72**, 40 (1998)
5. R-J. Xie, N. Hirosaki, M. Mitomo, K. Sakuma, N. Kimura, Appl. Phys. Lett. **89**, 241103 (2006)
6. B. Damilano, N. Grandjean, C. Pernot, Jpn. J. Appl. Phys. **40**, L918 (2001)
7. M.Yamada, Y. Narukawa, T. Mukai, Jpn. J. Appl. Phys. **41**, L246 (2002)
8. C.-F. Huang, C.-F. Lu, T.-Y. Tang, J.-J. Huang, C.C. Yang, Appl. Phys. Lett. **90**, 151122 (2007)
9. M. Funato, K. Hayashi, M. Ueda, Y. Kawaskami, Y. Narukawa, T. Mukai, Appl. Phys. Lett. **93**, 021126 (2008)
10. Y.Z. Xie, V.P. Kunets, Z.M. Wang, V. Dorogan, Y.I. Mazur, J. Wu, G.J. Salamo, Nano-Micro Lett. **1**, 1–3 (2009)
11. J. Wiersig, C. Gies, F. Jahnke, M. Aßmann, T. Berstermann, M. Bayer, C. Kistner, S. Reitzenstein, C. Schneider, S. Höfling, A. Forchel, C. Kruse, J. Kalden, D. Hommel, Nature **460**, 245 (2009)
12. D. Fattal, E. Diamanti, K. Inoue, Y. Yamamoto, Phys. Rev. Lett. **92**, 037904 (2004)
13. L.O. Mereni, V. Dimastrodonato, R.J. Young, E. Pelucchi, Appl. Phys. Lett. **94**, 223121 (2009)
14. S.J. Chua, C.B. Soh, W. Liu, J.H. Teng, S.S. Ang, S.L. Teo, Phys. Stat. Sol. (c) **5**, 2189 (2008)
15. H. Benisty, H.D. Neve, C. Weisbuch. IEEE J. Quantum Electron **34**, 1612 (1998)
16. C. Huh, K.S. Lee, E.J. Kang, S.J. Park, J. Appl. Phys. **93**, 9383 (2003)
17. M.R. Krames, M. Ochiai-Holcomb, G.E. Hofler, C. Carter-Coman et al., Appl. Phys. Lett. **75**, 2365 (1999)
18. H. Benisty, J-M. Lourtioz, A. Chelnokov, S. Combrie, X. Checoury, Proc. IEEE Recent Adv. Toward Optical Devices Semiconductor-Based Photonic Cryst. **94**, 997 (2006)
19. K. McGroddy, A. David, E. Matioli, M. Iza, S. Nakamura, S. DenBaars, J.S. Speck, C. Weisbuch, E.L. Hu, Appl. Phys. Lett. **93**, 103502 (2008)
20. P. Chen, A. Chen, S.J. Chua, J.N. Tan, Adv Mater. **19**, 1707 (2007)
21. W. Lee, R. Ji, U. Gösele, K. Nielsch, Nature Mat. **5**, 741 (2006)
22. K.Y. Zang, D.W.C. Cheong, H.F. Liu, H. Liu, J.H. Teng, S.J. Chua, Nanoscale Res. Lett. **5**, 1051–1056 (2010)
23. J.G. Lozano, A.M. Sánchez, R. García, S. Ruffenach, O. Briot, D. González, Nanoscale Res. Lett. **2**, 442–446 (2007)
24. C.B. Soh, W. Liu, J.H. Teng, S.Y. Chow, S.S. Ang, S.J. Chua, Appl. Phys. Lett, **92**, 261909 (2008)
25. T. Mukai, K. Takekawa, S. Nakamura, Jpn. J. Appl. Phys. Part 2 **37**, L839 (1998)
26. N. Grandjean, B. Damilano, J. Massies, S. Dalmasso, Solid Stat. Comms.**113**, 495 (2000)
27. M-K. Kwon, J-Y. Kim, II-K. Park, K.S. Kim, G-Y. Jung, S-J. Park, J.W. Kim, Y.C. Kim, Appl. Phys. Lett. **92**, 251110 (2008)